

# New isolates refine the ecophysiology of the Roseobacter CHAB-I-5 lineage

Victoria Celeste Lanclos<sup>1,5</sup>, Xiaoyuan Feng<sup>2,3</sup>, Chuankai Cheng<sup>1</sup>, Mingyu Yang<sup>4</sup>, Cole J. Hider<sup>1</sup>, Jordan T. Coelho<sup>1</sup>, Conner Y. Kojima<sup>1</sup>, Shelby J. Barnes<sup>1</sup>, Catie S. Cleveland<sup>1</sup>, Mei Xie<sup>2,3</sup>, Yanlin Zhao<sup>4</sup>, Haiwei Luo<sup>2,3</sup>, James Cameron Thrash<sup>1,\*</sup>

<sup>1</sup>Department of Biological Sciences, University of Southern California, Los Angeles, CA 90089, United States

<sup>2</sup>Simon F. S. Li Marine Science Laboratory, School of Life Sciences and State Key Laboratory of Agrobiotechnology, The Chinese University of Hong Kong, Shatin, SAR, Hong Kong, China

<sup>3</sup>Shenzhen Research Institute, The Chinese University of Hong Kong, Shenzhen, China

<sup>4</sup>Fujian Provincial Key Laboratory of Agroecological Processing and Safety Monitoring, College of Life Sciences, Fujian Agriculture and Forestry University, Fuzhou, China

<sup>5</sup>Present address: Department of Plant and Microbial Biology, University of California, Berkeley, Berkeley, CA, United States

\*Corresponding author. University of Southern California, Marine and Environmental Biology Section, Department of Biological Sciences, 3616 Trousdale Parkway, AHF 107, Los Angeles, CA 90089, USA. E-mail: thrash@usc.edu

## Abstract

The CHAB-I-5 cluster is a pelagic lineage that can comprise a significant proportion of all Roseobacters in surface oceans and has predicted roles in biogeochemical cycling via heterotrophy, aerobic anoxygenic photosynthesis (AAnP), CO oxidation, DMSP degradation, and other metabolisms. Though cultures of CHAB-I-5 have been reported, none have been explored and the best-known representative, strain SB2, was lost from culture after obtaining the genome sequence. We have isolated two new CHAB-I-5 representatives, strains US3C007 and FZCC0083, and assembled complete, circularized genomes with 98.7% and 92.5% average nucleotide identities with the SB2 genome. Comparison of these three with 49 other unique CHAB-I-5 metagenome-assembled and single-cell genomes indicated that the cluster represents a genus with two species, and we identified subtle differences in genomic content between the two species subclusters. Metagenomic recruitment from over fourteen hundred samples expanded their known global distribution and highlighted both isolated strains as representative members of the clade. FZCC0083 grew over twice as fast as US3C007 and over a wider range of temperatures. The axenic culture of US3C007 occurs as pleomorphic cells with most exhibiting a coccobacillus/vibrioid shape. We propose the name *Candidatus Thalassovivens* sp. nov., sp. nov. for the type strain US3C007<sup>T</sup> (= ATCC TSD-433<sup>T</sup> = NCMA B160<sup>T</sup>).

**Keywords:** CHAB-I-5; Roseobacter; bacterioplankton; marine microbiology; pangenomics; culturing; type strains

## Introduction

The Roseobacter group is one of the most ecologically successful groups of bacteria found across marine habitats and is often associated with phytoplankton blooms [1–4]. Members of this clade exist as free-living, attached, and in symbiont forms [1] and can make up to 20% of bacteria in coastal regimes [5]. The most abundant Roseobacters in the open ocean belong to the Pelagic Roseobacter Cluster (PRC), which are polyphyletic in the Roseobacter phylogenomic tree, but form a cluster in the dendrogram inferred from genome content similarity [3, 6, 7]. This results from multiple Roseobacter lineages that have evolved gene content that is adaptive for nutrient-poor pelagic waters, such as carbon monoxide and inorganic sulfur oxidation, use of dimethylsulfoniopropionate (DMSP) via multiple pathways, a reduction of metal import systems, and a high proportion of ABC transporters, some of which distinguish them from copiotrophic Roseobacters [6, 8, 9]. While many Roseobacter species are easily cultured, the PRC contains multiple clusters without currently isolated representatives, including the CHAB-I-5 lineage. Representatives from

the CHAB-I-5 cluster have been cultured on multiple occasions but lost [7, 10, 11], e.g. strain SB2 was the first [7].

The CHAB-I-5 cluster comprises free-living marine bacteria distributed from tropical to polar latitudes [7, 12] and is one of the most abundant types of Roseobacter in global oceans. It is found in highest abundances near coastal North America and Europe [12] and constituted up to 20% of microbial clones in the Sargasso Sea [1, 13]. In a study of Chesapeake Bay, CHAB-I-5 was the only Roseobacter that did not decrease in abundance along a salinity gradient and was present in samples across salinities from 13.9–30.5 [14]. While some other members of the Roseobacter group typically associate with phytoplankton blooms, this pattern does not seem to hold for CHAB-I-5 [7]. The abundance and distribution of CHAB-I-5 in global ocean waters corresponds to a high activity level in the cluster [1, 7, 12, 14, 15]. Furthermore, CHAB-I-5 phages are abundant in global waters, particularly in polar and estuarine systems [10]. This abundance, activity, and widespread phage distribution indicate this group is essential to global nutrient cycling, though the mechanisms of these dynamics are still unexplored.

Received: 28 May 2024. Revised: 10 March 2025. Accepted: 15 April 2025

© The Author(s) 2025. Published by Oxford University Press on behalf of the International Society for Microbial Ecology

This is an Open Access article distributed under the terms of the Creative Commons Attribution License (<https://creativecommons.org/licenses/by/4.0/>), which permits unrestricted reuse, distribution, and reproduction in any medium, provided the original work is properly cited.

Current predictions of CHAB-I-5 metabolism come from only four partial genomes [7, 12]. CHAB-I-5 appears to be motile with metabolic pathways for aerobic anoxygenic photosynthesis, carbon monoxide oxidation, inorganic sulfur oxidation, DMSP degradation, phosphonate metabolism, and evidence for thiamin and biotin auxotrophy similar to other PRC members [7, 9, 12]. Incomplete genomes have made it unclear whether CHAB-I-5 can use nitrate, nitrite, or reduce sulfur [7]. Furthermore, we have no knowledge of cell volumes, growth rates, or other fundamental physiological characteristics of this group. No CHAB-I-5 isolate has been maintained in culture long enough for experimental analysis except for the recent isolate FZCC0083, which remains uncharacterized except for use in phage isolations [10]. Thus, our current knowledge of CHAB-I-5 remains limited.

Here we present a new strain, US3C007, an axenic representative of the CHAB-I-5 cluster that is readily propagated on artificial seawater medium and reliably revived from frozen stocks. We conducted the first physiological characterization of CHAB-I-5, and the most extensive genomic analysis of the group to date using new, complete genomes from both US3C007 and FZCC0083 and other publicly available data. We showed the first morphology of a CHAB-I-5 member and examined the growth dynamics of both strains across ranges of salinity and temperature. Additionally, we analyzed the ecological distribution of CHAB-I-5 from an expanded set of global metagenomic samples that span a wide range of marine and estuarine locations. Together, these data constitute the most in-depth investigation of CHAB-I-5 thus far and provide new insights on the genomics and physiology of these organisms.

## Materials and methods

Note that for all software, default settings were used unless otherwise stated.

### US3C007 isolation

We obtained surface water (2 m) from the San Pedro Ocean Time series (SPOTs) monthly cruise on 09/16/2020 via CTD cast. The seawater was transported into the lab and filtered through a 2.7  $\mu\text{m}$  GF/D filter, stained with 1x Sybr green (Lonza) for 30 minutes in the dark, and cell density was enumerated on a Guava Easy Cyte 5HT flow cytometer (Millipore, Massachusetts, USA) with settings as described previously [16]. We diluted cells to a final concentration of 1 cell/ $\mu\text{l}$  in 10 ml of sterilized AMS1 artificial seawater medium [17] and inoculated 3  $\mu\text{l}$  of the diluted cell solution into each well of a 96  $\times$  2.1 ml well PTFE plate (Radleys, Essex, UK) containing 1.5 ml of AMS1 for a final theoretical concentration of 3 cells/well. Plates were incubated in the dark without shaking for 2.5 weeks and enumerated as described above. Positive wells ( $>10^4$  cells/ml) were transferred to Nalgene Oak Ridge PTFE centrifuge tubes (Thermo Fisher, Massachusetts, USA) containing MWH1 medium [18] in an attempt to move the cultures to a more frequently used medium for convenience. Subsequent transfers of isolates in MWH1 were not successful, so we transferred the initial cultures in the Oak Ridge tubes containing MWH1 to acid-washed 125 ml polycarbonate flasks containing the original isolation medium, AMS1, and growth resumed. The culture can be maintained in this manner over continual transfers. Cultures were cryopreserved in both 10% DMSO and 10% glycerol diluted with AMS1, however, we were only able to reproducibly revive these cultures from the cryostocks using glycerol. We grew US3C007 to late-log phase and filtered the cells onto a 0.2  $\mu\text{m}$  polycarbonate filter (Millipore) and extracted its

DNA using a GenElute Bacterial Genomic DNA Kit (Sigma-Aldrich Co, Darmstadt, Germany). We amplified the DNA and purified the PCR products as previously reported [19], and sent samples for Sanger sequencing to Genewiz (Azena Life Sciences, New Jersey, USA). We inspected the resulting chromatograms to verify purity through a lack of multiple peaks for a given base call, assembled a contiguous sequence from the forward and reverse complement sequences using CAP3 (<https://doua.prabi.fr/software/cap3>), and used the web-based NCBI BLASTn with the nr/nt database for sequence identification.

### 16S rRNA gene phylogeny to determine placement within CHAB-I-5

We created a 16S rRNA gene phylogeny to verify placement of US3C007 within the CHAB-I-5 cluster using the sequences and methods from a previous Alphaproteobacteria tree [18, 19], updated to include known CHAB-I-5 relatives including SB2 [7], three CHAB-I-5 SAGs [12], the original CHAB-I-5 clone [20], and our newly generated US3C007 sequence. We aligned sequences with muscle v3.8.1551 [21], trimmed with trimal v1.4.1 [22] with “-automated1”, and inferred the phylogeny with IQ-TREE v2.0.6 with flag “-B 1000” [23]. The phylogeny was visualized with Figtree v1.4.4 and all nodes were collapsed except for the branches containing CHAB-I-5 and PRC member HIMB11 to highlight US3C007’s inclusion within the CHAB-I-5.

### Genome sequencing and assembly

We revived US3C007 from cryostocks and grew the culture in multiple 1 L batches to gather DNA for genome sequencing. We filtered the cells onto 0.1  $\mu\text{m}$  polycarbonate filters (Millipore) and extracted DNA with a phenol chloroform approach (<https://www.protocols.io/view/modified-phenol-chloroform-genomic-dna-extraction-e6nvwkjzwvmk/v2>). DNA was pooled together and sent for Illumina NextSeq 2000 paired end (2x151bp) sequencing at the Microbial Genome Sequencing Center (MiGS) (Pittsburgh, USA). Illumina libraries were prepared with the Illumina DNA Prep kit and 10 bp UDI indices. Demultiplexing, quality control and adapter trimming was performed with bcl2fastq (v2.20.0422) ([https://support.illumina.com/sequencing/sequencing\\_software/bcl2fastq-conversion-software.html](https://support.illumina.com/sequencing/sequencing_software/bcl2fastq-conversion-software.html)). Illumina reads were trimmed using Trimmomatic (v0.38) (–phred33 LEADING:20 TRAILING:20 SLIDINGWINDOW:13:20 MINLEN:40) to remove poor quality bases [24]. We also performed long-read sequencing in-house using an Oxford Nanopore MinION with a R9.4.1 (FLOMIN106) flow cell (Oxford Nanopore, UK). For Nanopore sequencing, DNA was sheared with a size selection of 20 000 bp or greater using Covaris g-tubes (D-Mark Biosystems, Woburn, USA) and we constructed libraries with the SQK-LSK108 genomic DNA ligation kit (Oxford Nanopore, UK) with modifications (<https://doi.org/10.17504/protocols.io.bixskfne>). Reads were base-called with Guppy v4.4.1 [25], and demultiplexed using Porechop v0.2.4 (<https://github.com/rrwick/Porechop>). We assembled the long-read sequence data using Flye v2.9.1 [26] using the “nano-hq” setting and four rounds of polishing with minimap [27], included in the Flye assembler “–iterations 4”. We then used short reads from Illumina to further improve the assembly with Polypolish v0.5.0 [28]. The resulting assembly was visualized for completion with Bandage v0.8.1 [29].

Bacterial cultivation and DNA extraction of FZCC0083 were performed following our previous paper [10]. Briefly, a surface water sample was collected from the coast of the East China Sea. The FZCC0083 strain was isolated following the dilution cultivation procedure [11], and genomic DNA was extracted using

E.Z.N.A. kit (Omega Bio-tek, Norcross, USA). Library preparation and genome sequencing was performed following the standard protocols for Illumina sequencing on BGISEQ500 platform (PE100, Qingdao Huada Gene Biotechnology Co., Ltd) [30] and Nanopore sequencing on a Nanopore MinION sequencer (Oxford Nanopore Technologies Inc.) with a R9.4.1 (FLO-MIN106D) flow cell and the SQK-LSK109 genomic DNA ligation kit (Oxford Nanopore, UK). The Illumina sequencing reads (coverage >200x) were quality trimmed using Trimmomatic v0.36 [24] with options "SLIDINGWINDOW:4:15 MAXINFO:40:0.9 MINLEN:40". The Nanopore sequencing reads (coverage >700x) were base-called with Guppy v5.0.0 [25] via MinKNOW v21.11.8 and corrected using Necat v0.0.1 [31] with 'PREP\_OUTPUT\_COVERAGE=100 CNS\_OUTPUT\_COVERAGE=50' options then assembled using Flye v2.6 [26] with default parameters. The initial assembly was corrected using polished Nanopore sequencing reads by racon [32] twice with '-m 8 -x -6 -g -8 -w 500' options and the Illumina sequencing reads by Pilon v1.24 [33] three times with default parameters. The assembled contig was closed as validated using Bandage v0.8.1 [29].

## Taxon selection and phylogenomics

To expand the taxon selection for the CHAB-I-5 clade, we downloaded Rhodobacterales genomes from the NCBI and IMG databases (October, 2022), as well as large-scale metagenomic analyses including TARA Ocean [34, 35], BioGoShip [36], and OceanDNA [37]. First, a total of 259 genomes closely related to CHAB-I-5 (and a sister clade, represented by genomes like AG-337-I11 [38]) were selected based on having ANI values below 80% to other Roseobacters outside of these two groups. To categorically define the CHAB-I-5 cluster separate from the AG-337-I11 outgroup clade, 120 conserved bacterial single-copy genes were extracted and aligned using GTDB-tk v1.7.0 "classify\_wf" [39], and a phylogenetic tree was then constructed using IQ-TREE v2.2.0 [23] with parameters "-m LG+I+G -B 1000". We then dereplicated redundant CHAB-I-5 genomes using dRep v3.2.0 [40] with option "-pa 0.99 -ps 0.99", which sets average nucleotide identity at 99%. Genomes with higher estimated quality, which was defined as completeness minus five times the amount of contamination [41], were selected as representatives for the recruitment analysis. We also excluded one genome, OceanDNA\_b28631, because of its occurrence on a long branch in the phylogenomic tree and very low ANI (see below) to the remaining CHAB-I-5 genomes, which made its membership in this cluster questionable. The resulting set included 52 representative CHAB-I-5 genomes, which were used to build the final phylogenomic tree using the same approach described above. This phylogenomic tree was rooted using mad v2.2 based on minimal ancestor deviation approach [42]. This approach considers each branch as a possible root position, evaluates the ancestor-descendant relationships of all possible ancestral nodes in the tree, and chooses the branch with the minimal relative deviation as the root node [42].

## Comparative genomics

We compared the pairwise average nucleotide identity (ANI) with fastANI v1.33 [43] and visualized it in R. We used CheckM v1.1.3 "lineage\_wf" [41] to evaluate all genomes and the specific ssu\_finder function to identify the bacterial 16S rRNA genes. NCBI BLASTn was used for pairwise 16S rRNA gene comparisons. We also analyzed the metabolic potential of the final 52 genomes using Anvio' v7.1 [44] to generate predicted amino acid sequences from genome sequences and GhostKOALA [45] for annotation of the amino acid sequences with the KEGG orthology database [46]

using the same approach as we previously performed [47]. The resulting annotations and the original amino acid sequences were used with KEGG-Decoder and KEGG-Expander v1.3 [48] to catalog the metabolic pathways present. These metabolic annotations were further validated by comparing our orthologous groups with reference Roseobacter genomes (including Ruegeria pomeroyi DSS-3, *Dinoroseobacter shibae* DFL12, and *Planktomarina temperata* RCA23) using Orthofinder v2.2.1 [49].

## Metagenomic read recruitment

Using 1425 metagenomic samples from Yaquina bay [50], Sapelo Island [51], San Pedro Channel [52, 53], Baltic Sea [54, 55], Chesapeake Bay [56, 57], Columbia River [58], Black Sea [59], Gulf of Mexico [60], Pearl River [61], San Francisco Bay (SFB) [62], and the North Pacific Subtropical Gyre [63] along with globally distributed metagenomic datasets [64–68], we recruited reads to the CHAB-I-5 genomes using competitive read recruitment via RRAP [69] as previously reported [47] with default settings. Briefly, RRAP uses the latest versions of Bowtie2 [70] and SAMtools [71] to perform a competitive read recruitment from metagenomic samples to genomes, sort and index mapped reads, and normalize the data into RPKM values (Reads Per Kilobase (of genome) per Million (of recruited read base pairs)). We then analyzed the output in R. The OceanDNA\_b28631 was included in the recruitment with the other 52 genomes but excluded from visualization since we excluded it from our comparative genomics. We also examined whether there may have been bias in the read recruitment towards subsections of the genomes using the five top-recruiting genomes. We performed two analyses with a subset of metagenomes. First, we examined the relationship of RPKM to coverage for the top five genomes with the Pearl River and SFB datasets and calculated coverage with SAMtools after recruitment with RRAP as described above. Second, we compared the coverage fraction of the five genomes with the mean coverage for the Chesapeake Bay metagenomic reads using CoverM v0.4.0 "-p bwa-mem, -m covered\_fraction trimmed\_mean" [72].

## Microscopy

We initiated sample preparation by growing the US3C007 culture to a density of up to  $10^6$  cells/ml, ensuring they were in the exponential growth phase. Subsequently, we fixed the cells in 2.5% (final concentration) glutaraldehyde. To harvest the fixed cells, we passed 10 ml of the bacterial suspension through a 0.2  $\mu$ m Isopore polycarbonate filter (MilliporeSigma) coated with poly-L-lysine, facilitating cell adhesion to the filter membrane. Poly-L-lysine coating was achieved by immersing the membrane filter in a solution of Sigma P92155 at a concentration of 0.1 mg/ml. For cell membrane staining, we utilized a solution comprising 0.1 M HEPES buffered 0.05% Ruthenium Red (RuRed) with 10% sucrose. 10 ml of the RuRed solution was slowly passed through the filter, allowing for a 10-minute incubation period to ensure thorough staining. Then we performed a staining-fixing step using a solution containing 0.1 M HEPES buffered 0.05% RuRed, 0.8% Osmium tetroxide, and 10% sucrose. As in the previous step, 10 ml of the solution was slowly passed through the filter, with cells incubated for a minimum of 25 minutes. Following the staining-fixing process, we washed the membrane filter sequentially with two solutions: 10 ml of 0.1 M HEPES with 10% sucrose, followed by 10 ml of deionized water. Each washing step was carried out over a 10-minute duration. Subsequently, the samples underwent sequential dehydration in 50%, 70%, 95%, and 100% ethanol. The filter membrane was transferred to corresponding ethanol solutions in small containers and subjected to microwave treatment

for one minute in a laboratory microwave oven, maintaining a temperature below 40°C. Finally, the samples were preserved in 100% ethanol on the filter and stored at room temperature for further analysis. The filters were sputtercoated for 45 s with a Cressington 108 and imaged with the JSM-7001F-LV scanning electron microscope at the University of Southern California Core Center of Excellence in NanoImaging (<https://cni.usc.edu>). Resulting images were analyzed as described previously [47].

## Cell size analyses

Here we used a method adapted from previous studies [47]. Briefly, we segmented the cell image into two half spheres and a curved cylinder, mimicking a capsule geometry. The cell volume was then calculated as the sum of the volumes of the curved cylinder and the two half-spheres. While an ideal capsule assumes uniform radii for the half-spheres and the curved cylinder, variations in radii across different cell sections were addressed by measuring radii at multiple points and calculating geometric parameters (surface areas, volumes, lengths) based on each radius. Mean and median values of these parameters were used for visualization in our final violin plots.

We use Concepts for iPad v6.13 to measure to scale the image and to manually segment the cell area, measured in pixel squared (S). Additionally, the ruler feature in the application was employed to measure the radii of the cell by drawing circles covering widths at various sections, with each circle's radius recorded as "r". Mathematical equations for calculating surface areas (SA), volumes (V), lengths (l), and height (h) based on S and r are detailed in the supplemental figures. Our analysis encompassed the geometries of 24 cells where we also showcase the segmentations and circles drawn for measurements.

## Growth experiments

The carbon substrate experiment for US3C007 was completed first using modified versions of the isolation medium, AMS1, to adjust the carbon concentrations while keeping all other components of the isolation medium the same. We tested the following concentrations of carbon serving as the presumptive electron donor and carbon source: 0, 9.37, 18.8, 37.5, 75, 150, 300, and 600  $\mu$ M, as a 1:5:5 molar ratio mixture of methionine, glycine, and pyruvate. For better cell yields, we then further modified the media compositions in AMS1 and created a new recipe, CCM. In brief, the CCM media has no sulfate, completely relies on methionine for reduced sulfur, and has a 20X concentrated vitamin mix compared to AMS1. In addition, we substituted asparagine instead of glycine (which was added to aid in culturing SAR11 [17]) based on the genomic prediction of asparagine auxotrophy. We calculated the salinity of our media based on the chlorinity (salinity (ppt) =  $1.80655 \times Cl$  (ppt) [73]) of the "base salts". Although a small amount of chloride also comes from our nutrients (e.g. ammonium chloride as the nitrogen source, manganese chloride and nickel chloride in the trace metals), the concentrations were negligible, and we therefore did not incorporate those into the calculation of chlorinity. To test the salinity range of US3C0007, we made two batches of CCM at 0 and 50 ppt salinity and mixed them in different proportions to obtain the following salinities (ppt): 0, 5, 10, 15, 20, 25, 30, 35, 40, 45, and 49. The salinity experiment was conducted at 18.5°C (room temperature at that time). The temperature experiment was conducted using the CCM 30 ppt salinity medium at the following temperatures (°C): 4, 12, 16, 18.5, 21, 25, 28.5, 30, and 35.

For the carbon experiments, we counted cells with flow cytometry after staining with 1x Sybr green (Lonza 50513) for 30 minutes

in the dark. The carbon experiments were enumerated on the Guava Easy Cyte 5HT flow cytometer (Millipore, Massachusetts, USA) as described above, except for the third transfer (fourth growth cycle) of the carbon concentration experiment, which was enumerated with an Accuri C6 Plus (Becton Dickinson, New Jersey, USA). The cell signals on the flow cytometry were gated based on the scatter plot of forward scatter vs. green fluorescence area. For the salinity and temperature experiments, we stained the cells using a final concentration of 10X Sybr green in addition to 10X Tris-EDTA (Sigma-Aldrich T9285) and 0.25% glutaraldehyde (Sigma-Aldrich 354400). Tris-EDTA maintains the nucleotide staining reaction at pH 8. Glutaraldehyde helps fix the cells and permeabilize the membrane. Together with the more concentrated Sybr green, the additional pH buffer and fixative help improve the staining performance. For enumeration, we counted 30  $\mu$ l-100  $\mu$ l of sample/staining cocktail mixture using a medium flow rate (35  $\mu$ l/min, 15  $\mu$ m core size), threshold (triggering channel) of green fluorescence (533/30 nm) intensity at 1000. The cell signals were gated based on the green (533/30 nm) vs. yellow (585/40 nm) fluorescence intensity scatter plot. Based on the emission spectrum of Sybr green-stained DNA, we gated the signals with a ratio around 10:3 for green vs. yellow fluorescence intensities. We excluded autofluorescence signals from debris or media components, which usually have significantly higher yellow or red fluorescence compared to Sybr green-stained cells.

Culturing experiments for FZCC0083 were completed with an AMS1-based medium supplemented with a modified mixed carbon source [74], (1 $\times$  concentrations of carbon mixtures were composed of 0.001% [wt/vol] D-glucose, D-ribose, methionine, pyruvic acid, glycine, taurine, N-acetyl D-glucosamine, and 0.002% [vol/vol] ethanol). This medium was used at the following temperatures (°C): 4, 12, 16, 20, 24, 26, 30, 37. For the salinity experiment with FZCC0083, we used modified versions of AMS1 [17]. We kept the concentration of all added nutrient stocks constant and changed salinity by diluting or increasing the salt stocks while keeping the ratio of components constant. The exception to this was for sodium bicarbonate, which we kept constant to maintain buffering capacity. We tested the following salinities (ppt): 1, 2.3, 4.5, 9, 18, 22.6, 25.8, 30.1, 36, 43 at 24°C in the dark. Cells were enumerated on a Guava EasyCyte 5HT flow cytometer as described above.

## Growth curve analysis

Growth rates were calculated using a method adapted from our previously published sparse-growth-curve [75]. First, we applied a sliding window for every three time points and generated a linear regression of the time vs. log2 transformed cell densities using SciPy package (1.13.0). The slope of the linear regression gives us the instantaneous doubling rate. Next, to fully capture the uncertainties and variation of the statistics, we assigned each of the estimated slopes, plus and minus the standard deviation, to the start, middle, and end of the sliding window. This gave us nine candidate instantaneous doubling rates from any three time point cell densities. Since the end of a sliding window would become the middle of the next sliding window, and the start of the next, etc., each unique time point contributes to multiple estimated growth rates. We then took the median estimated growth rate for each unique time point. We used an automated method to identify the instantaneous growth rates belonging to exponential phase. We attempted to fit a sigmoid decay curve to the time vs. instantaneous doubling rate data with the expectation that the exponential phase would correspond to the period before the inflection point. If the curve fit failed, we took the top three

**Table 1.** CheckM genome statistics for the current and previously isolated strains.

Genome	Length (bp)	Scaffolds (circular)	N50 (bp)	GC %	Coding genes	Coding density	# rRNA gene operons	Reference
US3C007	3 622 411	1 (y)		50.7	3513	0.88	2	This study
FZCC0083	3 646 439	1 (y)		50.5	3564	0.88	2	This study
SB2	3 636 317	38 (n)	323 631	50.5	3527	0.89	1	[7]

instantaneous doubling rates with maximum absolute values. To demonstrate this growth rate calculation method, we have added an example iPython notebook at GitHub ([https://github.com/thrash-lab/insta\\_growth](https://github.com/thrash-lab/insta_growth)).

## Spectrophotometry

We attempted to measure bacteriochlorophyll in strain US3C007 via spectrophotometry of *in vivo* (whole cells) and pigment extracts. We performed direct *in vivo* measurements of culture volumes ranging from 50 ml to 1 L and cell densities from mid  $10^5$  to mid  $10^6$  cells/ml. Some runs involved filtering the cells onto sterile 0.1  $\mu\text{m}$  polyethersulfone (PES) Supor filters (PALL Corporation, Port Washington, NY, USA) or centrifugation of cells at 9000 rpm for 30 minutes. We used sterile CCM2 media for blanks and references. We also performed a washed cell-suspension using 950 ml of US3C007 culture filtered onto a sterile 0.1  $\mu\text{m}$  PES Supor filter with a 100 ml wash of carbonless artificial seawater media (YBC) [76] and resuspension in 2 ml of 1x PBS. In this case, 1x PBS was used as the reference and blank. For both *in vivo* approaches, cells were placed in a quartz cuvette (Hellma GmbH & Co. KG, Müllheim, DEU) and analyzed on a SpectraMax M2 plate reader (Molecular Devices, San Jose, CA, USA). The settings used were "Absorbance", 350–900 nm and 700–840 nm, to obtain a full and detailed spectra profile. We performed extract measurements by first filtering 500 ml of US3C007 culture ( $5 \times 10^{5-6}$  cells  $\text{ml}^{-1}$ , sterile 0.1  $\mu\text{m}$  PES Supor). Following previous methodology [77], the PES filter with the cells was extracted in 2 ml of 100% EtOH using the following minor modifications: PES filters were incubated for ~24 hours in sealed borosilicate glass tubes (VWR International LLC, Radnor, PA, USA). Following extraction, the 2 ml solution was then centrifuged at 5000 rpm for 5 minutes and 700  $\mu\text{l}$  of supernatant was placed in a quartz cuvette for analysis with the plate reader as described above. 100% EtOH was used as the blank and reference. All samples were kept in the dark or wrapped in foil to prevent BChla degradation.

## Results

### Isolation, identification, and genome sequencing

US3C007 originated from an untargeted dilution to extinction cultivation experiment inoculated with surface water collected from the San Pedro Ocean Time series (SPOT) monthly cruise on 16 September 2020. Its top 16S rRNA gene BLAST hit was 100% identity to Roseobacter sp. SB2, accession KX467571.1 (100% identity, 100% query coverage, accession length of 1343, and E-value of 0.0) [7]. The 16S rRNA gene phylogeny indicated US3C007 was the nearest phylogenetic neighbor to SB2 and the original clone library sequence of CHAB-I-5 [20] (Fig. S1). Strain FZCC0083 was isolated from the coastal waters of the East China Sea as previously described [10]. Hybrid long and short read genome sequencing resulted in single circularized contigs for both strains. Statistics for both genomes are reported in Table 1 in comparison

to the previously isolated strain SB2 [7]. All three strains have very similar sizes, GC content, and coding densities.

Phylogenomic analysis of 52 CHAB-I-5 genomes resulted in two subgroups, with US3C007 and SB2 on one branch and FZCC0083 on the other (Figs. 1A, S2–S3). We refer to these two branches as Subcluster 1 and Subcluster 2, respectively. Subcluster 1 had a minimum within-cluster average nucleotide identity (ANI) of 95.2%, whereas Subcluster 2 had a minimum within-cluster ANI of 94.5%. Between-cluster ANI percentages decreased below the species boundary, with a minimum of 90.6%, matching the phylogenomic branching pattern (Fig. 1). US3C007 and FZCC0083 both had two copies of the 16S rRNA gene. The two from US3C007 had 100% identity with SB2 (accession KX467571.1) and the two from FZCC0083 had 99.91% identity with SB2. The SB2 genome had only one copy of the rRNA gene operon located on a short contig, suggesting the other copy might not have assembled successfully. Comparisons of bulk genome characteristics across all 52 genomes showed a strong conservation of GC content ( $51.3 \pm 0.4\%$ ) and predicted coding density ( $89.3 \pm 0.9\%$ ) within CHAB-I-5 (Table S1).

### Biogeography

We mapped metagenomic reads to the CHAB-I-5 genomes from over fourteen hundred samples spanning a wide biogeography, including large ranges of salinity and temperature, to quantify CHAB-I-5 distribution. CHAB-I-5 was cosmopolitan, recruiting reads from around the globe. US3C007 was one of the top three most abundant representative genomes, including FZCC0083 and the ERR559527\_bin\_47\_MetaBAT\_v2\_12\_1\_MAG as the first and second most abundant, with AA076\_I17 and SB2 rounding out the top five (Fig. 2A). We observed recruitment across all latitudes and saw no specific relationship between genomes and latitude separate from that conferred by the locational bias of the samples themselves (Figs. S4–S5). Comparison of read recruitment with salinity demonstrated that all members of CHAB-I-5 prefer marine habitats, though some genomes do recruit limited numbers of reads from samples with a salinity as low as 8 (Figs. S5–S6). We also observed a tendency for genomes to recruit more reads from samples between temperatures of 11–20°C, even though most samples were from warmer locations (Figs. S5, S7). When abundance was summed by phylogenetic subcluster, the median recruited reads were smaller for Subcluster 1 than that of Subcluster 2 (Fig. 2B). However, Subcluster 1, containing isolates US3C007 and SB2, had a higher recruitment than Subcluster 2, the FZCC0083 type, at sites such as the Western United States coast, the Western South African coast, the North Sea, and the English Channel (Fig. 2B). Cluster 2 had higher recruitment at locations such as the Mediterranean, Pearl River, and much of the North Atlantic Gyre.

### Genomic content

We compared 52 non-redundant CHAB-I-5 genomes to determine the conservation of metabolic potential and whether the two

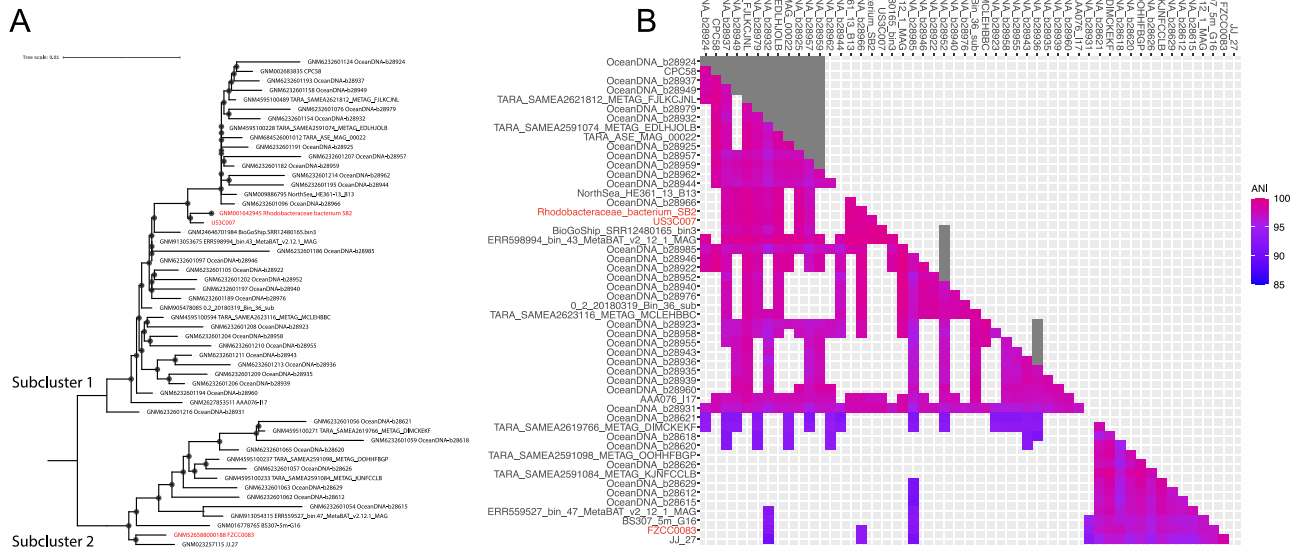


**Figure 1.** Phylogenomics and average nucleotide identity (ANI) of CHAB-I-5. **(A)** Phylogenetic tree of 52 CHAB-I-5 genomes rooted with minimal ancestor deviation. CHAB-I-5 isolates are highlighted in red and subclusters are labeled. Scale bar indicates changes per position. Filled circles indicate nodes with bootstrap values  $\geq 95\%$ . **(B)** Pairwise ANI of the CHAB-I-5 subclusters, colorized according to the key. Squares denoting 100% identity of each genome to itself are not colored.

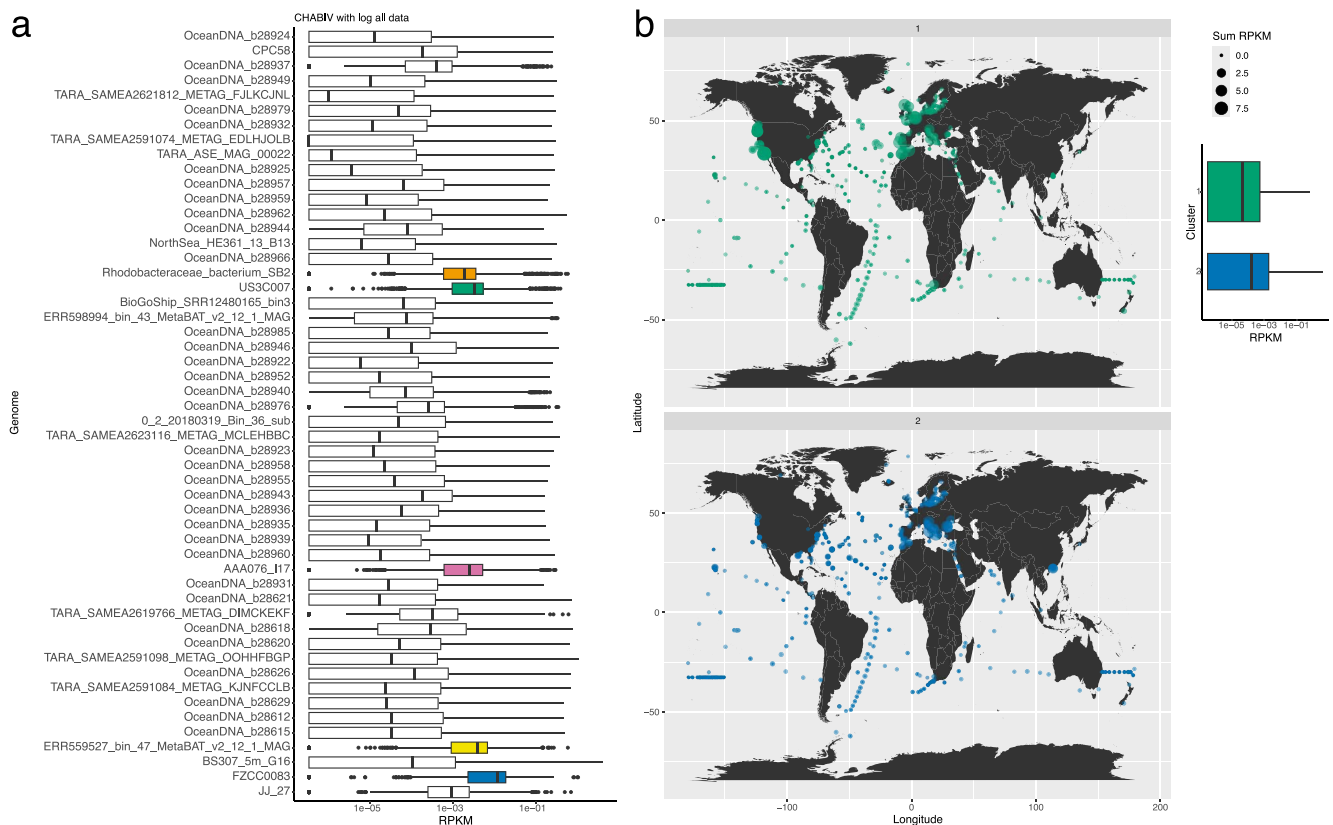


**Figure 2.** Biogeography and prevalence of CHAB-I-5 representatives. **(A)** Boxplots of all RPKM values for each genome in the analysis. Black lines within the boxes indicate median RPKM values. The top five recruiting genomes are colored. **(B)** Summed RPKM values for all genomes in each subcluster, plotted according to sample location. RPKM values are depicted by circle size according to the key. Boxplot indicates the range of values for all genomes in each subcluster.

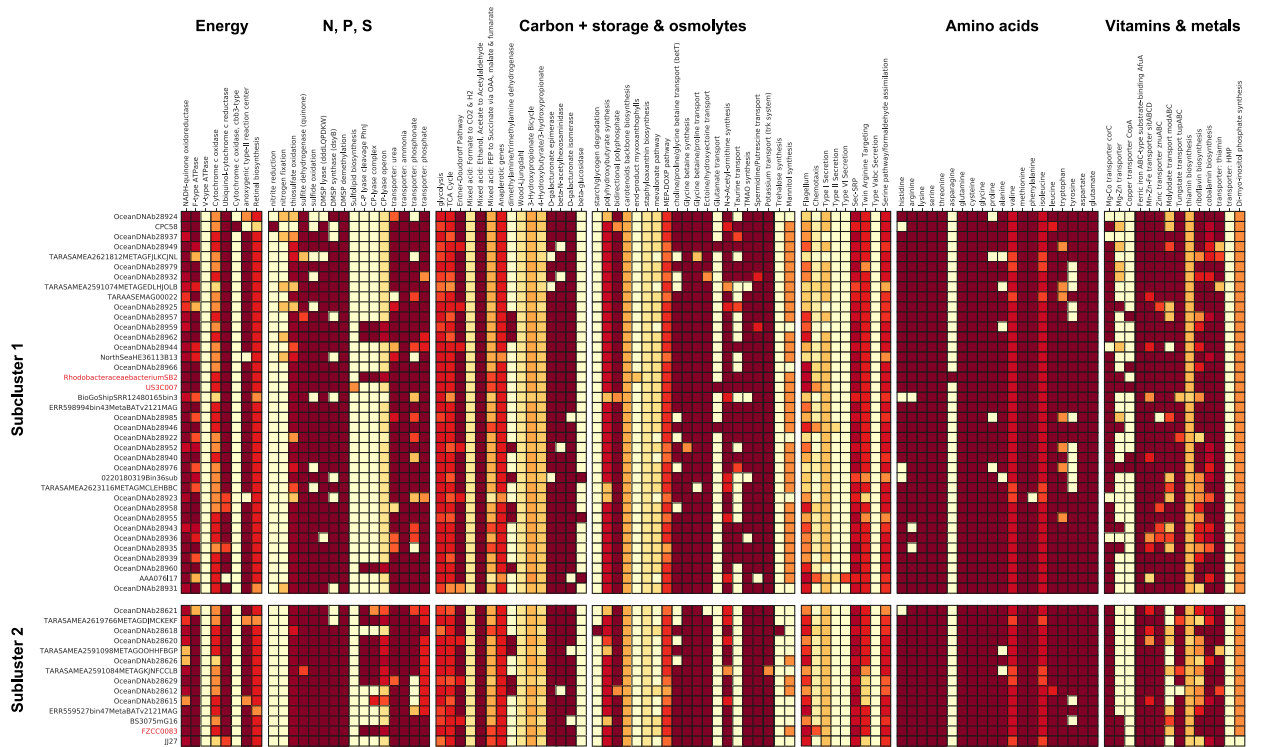


**Figure 3.** Predicted metabolism of CHAB-I-5. Subclusters are organized top to bottom to match the phylogeny of Fig. 2. Colors inside boxes correspond to pathway completion percentage according to the key. Genomes from isolates are noted in red.

subclusters could be distinguished genetically (Fig. 3, Table S1). Corroborating previous reports [7, 12], these organisms were predicted to be capable of aerobic chemoorganoheterotrophic metabolism with the potential for anoxygenic phototrophy. All the 52 non-redundant genomes had the potential for glycolysis via the Entner-Doudoroff pathway and the TCA cycle. All genomes contained nearly or fully complete electron transport pathways consisting of NADH-quinone oxidoreductases, F-type ATPases, cytochrome c oxidases, and ubiquinol-cytochrome c reductases. One genome, CPC58, contained a predicted *cbb<sub>3</sub>*-type cytochrome c oxidase. Most genomes had genes for polyhydroxyalkanoate (PHA) synthesis, a partial formaldehyde assimilation pathway, and a di/tri methylamine dehydrogenase. Most genomes had the potential to convert ethanol to acetate and acetaldehyde, and genes for anaplerotic C-fixation. Most genomes also contained a complete anoxygenic type-II reaction center. We found predicted genes for synthesis of bacteriochlorophyll a and/or b (*bchXYZ*, *bchC*, *bchF*, *chlG*, *chlP*- situated near the *puf* gene operon in US3C007) conserved across the CHAB-I-5 group, but found no annotated homologs for synthesis of bacteriochlorophyll d, c, or e. Full or partial pathways for flagella were also conserved.

Genes for metabolism of nitrogen, sulfur, phosphorous, trace metals, and vitamins were largely similar between subclusters. We found transporters for urea, ammonium, and phosphate were conserved, and most genomes contained a phosphonate transporter (Fig. 3). All 52 non-redundant genomes had the *napA* nitrate reductase, and CPC58 was the sole genome to encode a *nirK* nitrite reductase (Table S1). All genomes except for CPC58 contained nearly or full pathways for thiosulfate oxidation via the *sox* gene cluster, and a gene encoding a sulfite dehydrogenase quinone was conserved. All non-redundant genomes in Subcluster 1 and most in Subcluster 2 had genes for sulfide oxidation. Most genomes

had a DMSP lyase, all had genes for DMSP demethylation, and most genomes also encoded a DMSP synthase (Fig. 3, Table S1). Predicted urease genes were prevalent throughout both Subclusters. Several genomes also encoded the C-P lyase complex, operon, and cleavage potential, although the latter was more common in Subcluster 2, and the US3C007 genome did not encode for the C-P lyase. Most genomes had a predicted Mg-Co transporter, Mg-Zn transport potential, and some genomes in Subcluster 1, including US3C007, had a *copA* copper transporter (Fig. 3, Table S1). Most genomes had ferric iron, Mn-Zn-Fe, zinc, and tungstate transporters. Most genomes in Subcluster 1 contained partial or nearly complete pathways for molybdate transport whereas only one genome in Subcluster 2 contained at least a half pathway. No genome contained the full pathway for thiamin biosynthesis, though a partial pathway was common. Most genomes contained either a full or partial pathway for riboflavin and cobalamin biosynthesis and thiamin transport.

Amino acid metabolism was also very similar between subclusters. Prototrophy for lysine, serine, threonine, glutamine, histidine, arginine, cysteine, glycine, valine, methionine, isoleucine, tryptophan, aspartate, and glutamate was largely conserved, whereas asparagine auxotrophy was widespread (Fig. 3). Glycine betaine synthesis, glycine betaine/proline transport, and ectoine/hydroxyectoine transport were also conserved. Most genomes in Subcluster 1 could transport taurine, whereas none of the non-redundant genomes from Subcluster 2 contained this pathway, including the complete genome of FZCC0083 (Fig. 3, Table S1).

Thus, the genome content across both subclusters was quite similar. The notable differences between the subclusters were the presence of the taurine and copper transporters as well as *pcAGH* dioxygenase genes exclusively within Subcluster 1, a greater prevalence of C-P lyase genes and low affinity phosphate transporter in Subcluster 2. Therefore, the Subclusters within

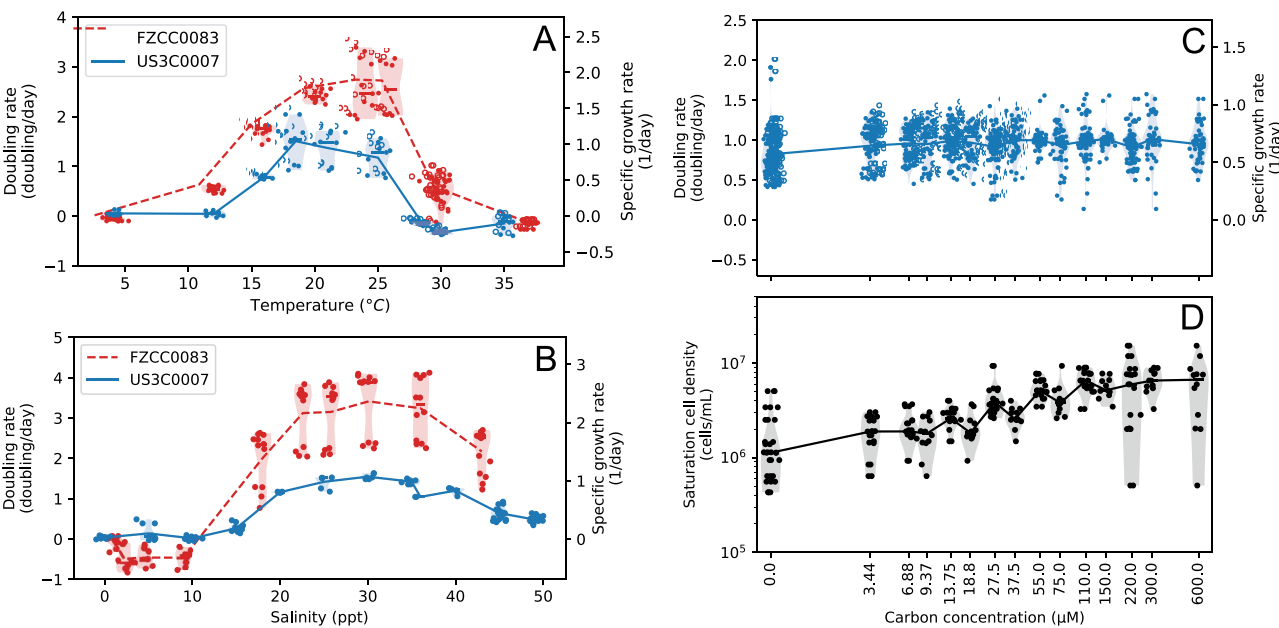


**Figure 4.** Growth rates for US3C007 and FZCC0083 across (A) temperatures, (B) salinities, and for US3C007 (C) at differing low carbon concentrations. (D) Growth yields for US3C007 under the same carbon experiments for C. Data in (A–C) comes from instantaneous growth rates throughout exponential phase. Data points are plotted along with medians (lines) and the distribution (violin plot shaded region).

CHAB-I-5 may exhibit some niche differentiation based on dissolved organic nitrogen and phosphorus utilization.

### Physiology and morphology

US3C007 grew consistently between 16–25°C, but not at temperatures of 12°C or below, or at 28.5°C or above (Figs. 4A, S8). Additionally, US3C007 grew at salinities of 15–49 ppt, but not at 10 ppt or below (Figs. 4B, S8). The maximum observed growth rate was  $1.55 \pm 0.05$  divisions day $^{-1}$  at 18.5°C and 30 ppt (Fig. 4B; Table S1). We tested US3C007's growth across a range of carbon concentrations to determine the carbon concentration to which it was best adapted. The primary carbon sources in the carbon mix were methionine, glycine, and pyruvate at a 1:5:5 molar ratio. We tested eight concentrations up to 600  $\mu$ M carbon, with 300  $\mu$ M carbon being the concentration in AMS1 medium (resulting from 10  $\mu$ M methionine, 50  $\mu$ M glycine, and 50  $\mu$ M pyruvate) (Table S1). We observed no net change in growth rate with increasing carbon concentration, but an increase in yield (Figs. 4C–D, S8). The consistent growth rate at low carbon concentrations indicates that this strain is particularly well adapted to low carbon environments. However, even after three transfers (four total growth cycles from lag to late log or stationary phase), we observed continued growth in the negative control, (Fig. 4C), albeit to lower cell densities than those cultures receiving carbon additions (Fig. 4D). We hypothesize this growth resulted from the strain having genes for PHA storage (Fig. 3), but this remains to be tested. We attempted to measure bacteriochlorophyll in whole cells but were unable to determine a definitive spectrophotometric peak. This could have been the result of inadequate biomass or growth conditions that did not lend themselves to bacteriochlorophyll production.

FZCC0083 grew considerably faster than US3C007 in all conditions tested (Figs. 4A–B, S8; Table S1). The maximum observed growth rate was  $3.41 \pm 0.44$  divisions day $^{-1}$  at 24°C and 30.1 ppt (Fig. 4B)– more than twice the division rate of US3C007. FZCC0083 had a wider temperature growth envelope than US3C007, growing between 12–30°C with no growth at 4°C or 37°C. Its salinity tolerance was like that of US3C007, growing between 18–43 ppt, but not

at 9 ppt or below. Thus, these two strains have notable differences in physiology which reflects their phylogenetic separation (Fig. 1).

US3C007 cells were small, having average cell lengths  $\sim 1.65 \mu$ m and radii  $\sim 0.23 \mu$ m, yielding cell volumes  $\sim 0.44 \mu\text{m}^3$  (Fig. 5A). We observed multiple morphologies within a single clonal culture (Figs. 5B–E, S9–S10). Single cells were usually bacillus-shaped, with some displaying more curved rod morphology or bulbous coccobacillus shapes (Fig. 5B–E, S9–S10).

### Discussion

This study is the most comprehensive analysis of the CHAB-I-5 subcluster within the larger “Roseobacter” group of Rhodobacterales to date. We have expanded the genomic and ecological characterization from four to 52 unique CHAB-I-5 genomes, including the first two circularized CHAB-I-5 genomes, and two new, publicly available CHAB-I-5 isolates, strains US3C007 and FZCC0083. Both strains are reliably propagated in artificial seawater media that are easily modified and we provided the first physiological and morphological characterization for members of the CHAB-I-5 group. Our expanded analysis also took advantage of recently generated, publicly available CHAB-I-5 genomes to understand intra-clade genomic diversity using phylogenomics and ANI. A prior study established two subclusters within CHAB-I-5 using environmental 16S rRNA gene sequence phylogeny [7], and we see the same division in our analysis. Both phylogenomics and average nucleotide identity support at least two subgroups within CHAB-I-5, denoted Subcluster 1 and Subcluster 2, that represent two species within a genus based on within- and between-subcluster ANI (Fig. 1). Isolate US3C007 belongs to Subcluster 1 and isolate FZCC0083 belongs to Subcluster 2.

Metabolic potential within CHAB-I-5 was highly conserved (Fig. 3). Nevertheless, we observed a few differences between Subclusters that may point to specific metabolic adaptations. The taurine ABC transporter tauABC was present in Subcluster 1 and not Subcluster 2 is (Fig. 3). Taurine is an important, multifunctional compound that serves as an osmoregulation

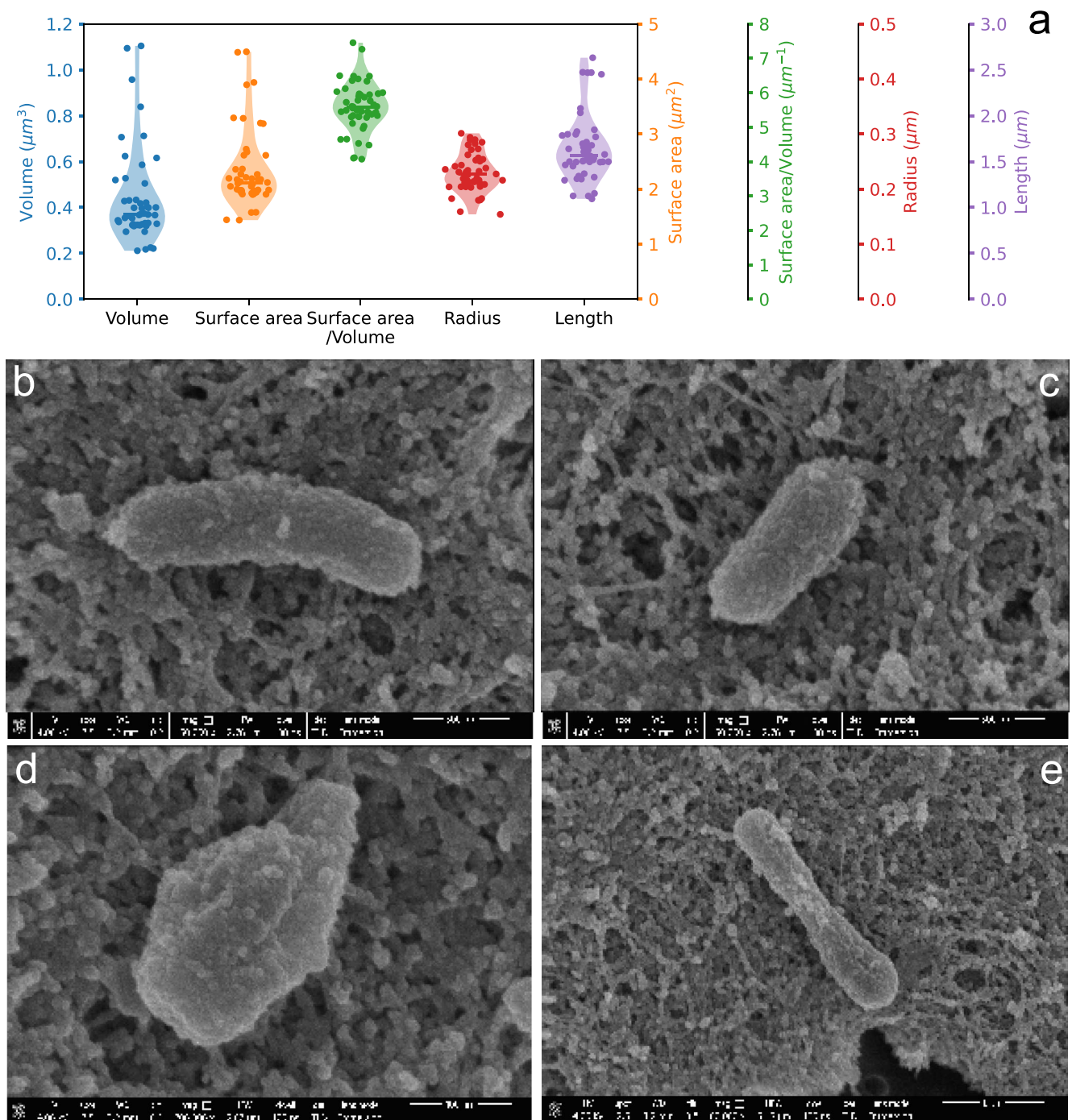


**Figure 5.** Cell size and shape of US3C007. **(A)** Dimensions from analysis of 24 separate cells (see Figs. S9, S10) of different sizes and shapes. Medians are indicated with a bar and the violin plot shading shows the distribution of the data. **(B-E)** representative cells of different size/shape configurations seen in the culture. Scale bars (500 nm B, C; 400 nm D; 1  $\mu\text{m}$  E) are indicated below each image.

tool and as a source for carbon, nitrogen, and sulfur for marine bacteria [78]. This differential ability to transport taurine may confer a growth advantage for Subcluster 1, but future research is needed to confirm how taurine is used, as all genomes encoded pathways for taurine catabolism, and the fewer number of genomes in Subcluster 2 may have biased this view. Another notable difference in metabolic content between the CHAB-I-5 subclusters was that of the C-P lyase genes. C-P lyases cleave carbon-phosphorous bonds and are used as a phosphate scavenging strategy that produces methane aerobically [79, 80]. Although all strains had typical *pstABCS* phosphate transporters,

Subcluster 2 was enriched in C-P lyase genes, while only a few Subcluster 1 genomes had the pathway (Fig. 3). These results suggest Subcluster 2 interacts more consistently with the dissolved organic phosphorous pool and may contribute to methane production in global oceans. A subset of genomes in Subcluster 1 also contained the *copA* copper transporter exclusively, including US3C007, but distribution was spotty, suggesting a lack of conservation for the use of copper and/or that we didn't observe the gene due to incomplete genomes.

We also extended the analysis of CHAB-I-5 distribution through read recruitment from over fourteen hundred metagenomic

samples, including those in brackish and freshwater environments. Our results expand the known ecological distribution of CHAB-I-5 members, showing their presence in sample sites such as the North Atlantic gyre, South Pacific, Gulf of Mexico, Red Sea, and polar locations that were unavailable or had fewer sites surveyed in previous reports of CHAB-I-5 biogeography (Fig. 2) [7, 12]. Our work confirms and extends the view of CHAB-I-5 as a cosmopolitan member of the global oceans, and although the Sub-clusters were generally found in all the same locations, there were some samples where one Subcluster dominated (Fig. 2B). Subcluster 2 recruited more overall reads than Subcluster 1 (Fig. 2B), and the FZCC0083 and US3C007 genomes recruited the first and third most reads across all the samples (Fig. 2A). We performed spot checks of the relationship between coverage and abundance to explore whether recruitment was biased to conserved genomic content. In cases where the top-recruiting genomes were rare, the coverage of those genomes was low, however, the reverse was also true: coverage was generally proportional to abundance, and thus we don't believe that read recruitment was biased to specific regions of the genome (Fig. S12). Together, our results suggest that these genomes are highly representative of CHAB-I-5 across the global oceans and make the strains excellent candidates for further study of the clade.

CHAB-I-5 can be abundant and active in polar latitudes [7, 12], however, our data did not show strong evidence of latitudinal preferences by genome (Fig. S4). Our initial physiological findings demonstrated restricted temperature range for both strains, representing each subcluster. US3C007 grew between 16°C and 28.5°C and FZCC0083 grew between 12°C and 30°C. These ranges are narrower than the observed range in metagenomic data for each genome, which both had substantial read recruitment in samples where the water temperatures were below 10°C (Fig. S7). This suggests the presence of (still uncultured) strains closely related to US3C007 and FZCC0083 with greater psychrotolerance. In fact, many of the other SAG/MAG CHAB-I-5 genomes showed maximum read recruitment in samples below 15°C (Fig. S6), so it is likely that multiple strains of CHAB-I-5 are better cold-adapted than the two isolates.

On the other hand, the discrepancy between the lab and field measurements for US3C007 and FZCC0083 could describe the difference between realized and fundamental niches. Although the ideal fundamental niche space is sometimes envisioned as more extensive than the realized niche [81, 82], the reverse can also be true. For example, multiple ecotypes of *Prochlorococcus* had narrower temperature growth ranges in the laboratory than the ranges observed in nature via molecular data [83]. This is like the pattern we observed in both US3C007 and FZCC0083, where the realized niche appears larger than the fundamental niche with regards to temperature (Figs. 4, S4). For *Prochlorococcus*, the authors considered that a cultivation bias, stemming from continual maintenance of cultures in a restricted temperature range, could have led strains to evolve a different temperature optimum than the original population [83]. Similarly, continual culturing could also lead strains to evolve a narrower temperature tolerance than would have been maintained by strains in the fluctuating natural environment. This would result in a contraction of the measured fundamental niche relative to the realized niche. However, another plausible explanation was that dispersal of *Prochlorococcus* resulted in cells being distributed to many locations outside their optimal temperature range [83]. Since our culture experiments are regularly restarted from cryopreserved samples, it was unlikely that our strains had evolved a more restricted temperature range since their isolation. Therefore, we consider

our observations of a wider realized niche than fundamental niche to be consistent with the dispersal hypothesis as well.

Regarding the relationship with salinity, our experiments suggested that CHAB-I-5 is an exclusively marine organism (Fig. 4B). Our read recruitment agreed—no genomes showed strong preferences for brackish or freshwater habitats (Figs. S5, S7). This is consistent with the fact that CHAB-I-5 appears to constitute a genus. In other abundant free-living microbial groups like SAR11 and Aegean-169 that have subclades adapted to lower salinities, those subclades circumscribe a similar taxonomic breadth as that of CHAB-I-5 [47, 84], so we would not necessarily expect to see adaptation for specific salinities within CHAB-I-5. That said, other Roseobacter relatives have been isolated from brackish salinities [18, 19, 85, 86], and CHAB-I-5 members have been observed in equivalent abundances along the salinity gradient of the Chesapeake Bay [14]. While we found no clear evidence of fresh or brackish water specialists within CHAB-I-5, multiple genomes did recruit low numbers of reads from brackish waters with salinities as low as 8 (Fig. S5). Future work measuring activity of CHAB-I-5 across salinities could provide insight to whether the cells might be active in these lower salinity environments, and/or whether true brackish water-adapted strains exist.

The US3C007 and FZCC0083 cultures have provided the first growth and morphological data for CHAB-I-5. These cultures span a wide range of growth rates, with the maximum for FZCC0083 being over twice as fast as that of US3C007 (3.41  $\pm$  0.44 vs. 1.55  $\pm$  0.05 divisions day $^{-1}$ ). These phenotypic differences likely reflect that these are different species, isolated from different oceanic regimes. Strain US3C007 was isolated from surface water collected at SPOT, a unique temperate semi-coastal location between Catalina Island and the coast of California overlying the San Pedro Basin at nearly 900 m depth. Water circulation patterns in the Southern California Bight are complex [87, 88], but SPOT is inshore of the California Current system and average fall surface temperatures (warmest of the year) in the nearby Santa Monica Basin can reach 20.5°C [89]. Conversely, strain FZCC0083 was isolated from coastal waters off Pingtan Island, in the shallow Taiwan Strait very near the delineation of the East and South China Seas [10]. This location is in shallow water (< 30 m) and over 8 degrees of latitude south of SPOT (~900 km). Regional currents in this area branch from the Kuroshio Current system and fall average surface temperatures can reach 26°C [90]. Minimum temperatures in both areas are near 14°C. The optimization of FZCC0083 for growth at higher temperatures than US3C007, as well as the ability of FZCC0083 to grow at higher maximum temperatures (Fig. 4A), likely reflects the higher average temperatures in the Taiwan Strait compared to the Southern California Bight. Overall relative abundances of Subcluster 1 (US3C007-type) and Subcluster 2 (FZCC0083-type) with temperature were subtle but showed general trends that match the isolate physiology: both trended downward with temperature, but Subcluster 1 had a slightly more negative correlation (Fig. S11). Thus, the growth physiology may signify larger habitat preferences for the Subclusters.

The considerable differences in growth rate between the two strains suggests more complex evolutionary diversification acting on multiple aspects of cell physiology. Nevertheless, the growth rates of these two strains span that of others in the larger PRC. Division rates for the model Roseobacter group organism, *R. pomeroyi* DSS-3 $T$ , which is not a PRC member, have been reported at up to 9.6 day $^{-1}$  [91]. The PRC includes many organisms with distinct genomic and lifestyle differences from better-studied copiotrophic Roseobacter group members like *R. pomeroyi* [7, 9, 92]

and there are a few examples of cultured representatives from the PRC. Isolates from the DC5-80-3 (also called RCA) and CHUG groups that accompany CHAB-I-5 in the PRC have yielded some important growth insights [9, 93–95]. Strain LE17 had division rates of roughly 2–3 day<sup>-1</sup> [94], and strain HKCCA1288 had division rates closer to 2 day<sup>-1</sup> [9], although optimized medium has reduced this to just under 5 hours (4.8 day<sup>-1</sup>) [91]. The type strain for the DC5-80-3 cluster, *Planktomarina temperata* RCA23<sup>T</sup>, as well as another close relative of US3C007, strain HIMB11, grew preferentially at mesophilic temperatures like US3C007 [93, 96], and the maximum observed growth rate of *P. temperata* RCA23<sup>T</sup> was very close to 1 day<sup>-1</sup> [97]. Given the close relationship between them, the variation in growth rates between US3C007 and FZCC0083 provide an excellent opportunity to investigate fundamental limits on growth rate. More strains from different locales will be important for exploring phenotypic heterogeneity within the group.

Our microscopic observation of strain US3C007 revealed significant pleomorphism in the culture (Fig. 5B–E). Pleomorphism and irregular morphology has been recorded in other Roseobacter group members, including HIMB11 [96]. Both HIMB11 and US3C007 have cells that are coccobacillus as well irregular rods [96] (Fig. 5B–E). The weighted average cell volume of 1276 heterotrophic cells across 23 coastal ocean samples was  $0.11 \pm 0.17 \mu\text{m}^3$  [98], whereas average US3C007 volume was  $0.44 \pm 0.06 \mu\text{m}^3$  across a variety of morphologies (Fig. 5A). Thus, US3C007's average cell volume is greater than the average heterotrophic bacterium, stemming in part from a relatively large radius for the cell length, compared to cells like that of SAR11 [47, 99, 100]. Future work to determine the extent of morphological variation and its drivers in natural populations of CHAB-I-5 will be important to understand the biology of these organisms more generally and for modeling the impact of carbon cycling by CHAB-I-5.

Overall, this work provides the most comprehensive genomic and ecological characterization of CHAB-I-5 to date and the first physiological data for the group. These recent advances in the availability of public CHAB-I-5 genomes and a new isolate that is representative of the CHAB-I-5 in global waters is a crucial component needed to characterize this abundant and highly active fraction of the microbial community. Future work is needed on US3C007 and the CHAB-I-5 cluster that could include comparative physiology between FZCC0083 and US3C007 to highlight whether a growth advantage might be conferred in the environment based on phosphorous, copper, or taurine availability and to quantify global estimates of CHAB-I-5's contribution to biogeochemical cycling in the oceans.

We have deposited strain US3C007 into two culture collections to promote additional research on the group and propose a new name for the strain below. We note that the originally proposed *Candidatus* name, “*Candidatus Planktomicrobium forsetii*” [7], was an orthographic variant of the existing genus *Planctomicrobium* [101]. Thus we have chosen a new designation for the group.

## Description of *Candidatus Thalassovivens*, gen. nov.

*Thalassovivens* (*Tha.las.so.vi*'vens. Gr. fem. n. *thalassa*, the sea; L. pres. part. *vivens*, living, N.L. fem. n. *Thalassovivens*, an organism living in the sea, in reference to the marine habitat of these organisms).

Aerobic, with chemoorganoheterotrophic, chemolithotrophic, and anoxygenic phototrophic metabolisms. Encodes genes for

glycolysis through the Entner-Doudoroff pathway and the TCA cycle. Genome sizes of ~3.6 Mbp, with GC content ~51% and a coding density ~89%. Prototrophy predicted for lysine, serine, threonine, glutamine, histidine, arginine, cysteine, glycine, valine, methionine, isoleucine, tryptophan, aspartate, and glutamate, with asparagine auxotrophy. Glycine betaine synthesis, glycine betaine/proline transport, and ecotine/hydroxyectoine transport genomically conserved. Genes for the PII nitrogen regulatory system, *ntrXY*, *amtB*, and urease conserved. Most genomes also encode genes for aerobic vitamin B<sub>12</sub> synthesis. Genes for synthesis of bacteriochlorophyll a and/or b conserved. Motility via flagella is predicted.

## Description of *Candidatus Thalassovivens* sp. nov.

*Thalassovivens* sp. nov. (sp'o'tae. N.L. gen. n. *spotae*, in reference to the San Pedro Ocean Time series (SPOT), from which the strain was isolated).

In addition to the characteristics of the genus, it has the following features. Cells are coccobacillus shaped, pleomorphic, with average dimensions of 0.23  $\mu\text{m}$  radius, 1.65  $\mu\text{m}$  length, and 0.44  $\mu\text{m}^3$  volume. Halophilic, growing in salinities of 15–49 ppt, but not at 10 ppt or below. Mesophilic, growing between 16–25°C, but not at temperatures of 12°C or below, or at 28.5°C or above. Has a maximum growth rate of 1.55  $\pm$  0.05 divisions day<sup>-1</sup> at 20°C and salinity of 30 ppt.

The type strain, US3C007 (= ATCC TSD-433<sup>T</sup> = NCMA B160<sup>T</sup>), was isolated from surface water (2 m) collected at the San Pedro Ocean Time series (33°33' N, 118°24' W). The genome sequence is circularized at 3622411 bp with 50.7% GC content. The genome is available on NCBI at BioProject number PRJNA1044073.

## Acknowledgements

We thank Dr. Aharon Oren for assistance with nomenclature and acknowledge the Center for Advanced Research Computing at the University of Southern California for providing computing resources that have contributed to the research results reported within this publication (<https://cacr.usc.edu>).

## Supplementary material

Supplementary material is available at ISME Communications online.

## Conflicts of interest

The authors declare no competing financial interests.

## Funding

This work was supported by a Simons Early Career Investigator in Marine Microbial Ecology and Evolution Award, and NSF Biological Oceanography Program OCE-1945279 and Emerging Frontiers Program EF-2125191 grants to J.C.T.

## Data availability

The genome sequences and raw reads for strains US3C007 and FZCC0083 can be found at NCBI under BioProject numbers PRJNA1044073 and PRJNA1047292, respectively. Supplementary material, including scripts, tree files, and Table S1, can be found

on FigShare (<https://doi.org/10.6084/m9.figshare.25898389>). The type strain, US3C007<sup>T</sup>, is available at the American Type Culture Collection and the Bigelow National Center for Marine Algae and Microbiota (= ATCC TSD-433<sup>T</sup> = NCMA B160<sup>T</sup>), as well as from the Thrash Laboratory upon request.

## References

1. Buchan A, González JM, Moran MA. Overview of the marine roseobacter lineage. *Appl Environ Microbiol* 2005; **71**:5665–77. <https://doi.org/10.1128/AEM.71.10.5665-5677.2005>
2. Buchan A, LeCleir GR, Gulvik CA. et al. Master recyclers: features and functions of bacteria associated with phytoplankton blooms. *Nat Rev Microbiol* 2014; **12**:686–98. <https://doi.org/10.1038/nrmicro3326>
3. Simon M, Scheuner C, Meier-Kolthoff JP. et al. Phylogenomics of Rhodobacteraceae reveals evolutionary adaptation to marine and non-marine habitats. *ISME J* 2017; **11**:1483–99. <https://doi.org/10.1038/ismej.2016.198>
4. Liang KYH, Orata FD, Boucher YF. et al. Roseobacters in a sea of poly- and Paraphyly: whole genome-based taxonomy of the family Rhodobacteraceae and the proposal for the split of the 'Roseobacter clade' into a novel family, Roseobacteraceae fam. Nov. *Front Microbiol* 2021; **12**:683109. <https://doi.org/10.3389/fmicb.2021.683109>
5. Moran MA, Belas R, Schell MA. et al. Ecological genomics of marine Roseobacters. *Appl Environ Microbiol* 2007; **73**:4559–69. <https://doi.org/10.1128/AEM.02580-06>
6. Luo H, Löytynoja A, Moran MA. Genome content of uncultivated marine Roseobacters in the surface ocean: genome content of wild Roseobacters. *Environ Microbiol* 2012; **14**:41–51. <https://doi.org/10.1111/j.1462-2920.2011.02528.x>
7. Billerbeck S, Wemheuer B, Voget S. et al. Biogeography and environmental genomics of the Roseobacter-affiliated pelagic CHAB-I-5 lineage. *Nat Microbiol* 2016; **1**:16063. <https://doi.org/10.1038/nmicrobiol.2016.63>
8. Luo H, Moran MA. Evolutionary ecology of the marine Roseobacter clade. *Microbiol Mol Biol Rev* 2014; **78**:573–87. <https://doi.org/10.1128/MMBR.00020-14>
9. Feng X, Chu X, Qian Y. et al. Mechanisms driving genome reduction of a novel Roseobacter lineage. *ISME J* 2021; **15**:3576–86.
10. Zhang Z, Wu Z, Liu H. et al. Genomic analysis and characterization of phages infecting the marine Roseobacter CHAB-I-5 lineage reveal a globally distributed and abundant phage genus. *Front Microbiol* 2023; **14**:14. <https://doi.org/10.3389/fmicb.2023.1164101>
11. Yang S-J, Kang I, Cho J-C. Expansion of cultured bacterial diversity by large-scale dilution-to-extinction culturing from a single seawater sample. *Microb Ecol* 2016; **71**:29–43. <https://doi.org/10.1007/s00248-015-0695-3>
12. Zhang Y, Sun Y, Jiao N. et al. Ecological genomics of the uncultivated marine Roseobacter lineage CHAB-I-5. *Appl Environ Microbiol* 2016; **82**:2100–11. <https://doi.org/10.1128/AEM.03678-15>
13. Venter JC, Remington K, Heidelberg JF. et al. Environmental genome shotgun sequencing of the Sargasso Sea. *Science* 2004; **304**:66–74. <https://doi.org/10.1126/science.1093857>
14. Buchan A, Hadden M, Suzuki MT. Development and application of quantitative-PCR tools for subgroups of the Roseobacter clade. *Appl Environ Microbiol* 2009; **75**:7542–7. <https://doi.org/10.1128/AEM.00814-09>
15. Henriques IS, Almeida A, Cunha A. et al. Molecular sequence analysis of prokaryotic diversity in the middle and outer sections of the Portuguese estuary ria de Aveiro. *FEMS Microbiol Ecol* 2004; **49**:269–79. <https://doi.org/10.1016/j.femsec.2004.04.003>
16. Thrash JC, Weckhorst JL, Pitre DM. Cultivating fastidious microbes. In: TJ M.G., Timmis K.N., Nogales B. (eds.), *Springer Protocols Handbooks*. Berlin, Heidelberg: Springer Berlin Heidelberg, 2015, 57–78.
17. Carini P, Steindler L, Beszteri S. et al. Nutrient requirements for growth of the extreme oligotroph 'Candidatus Pelagibacter ubique' HTCC1062 on a defined medium. *ISME J* 2013; **7**:592–602. <https://doi.org/10.1038/ismej.2012.122>
18. Henson MW, Lanclos VC, Pitre DM. et al. Expanding the diversity of Bacterioplankton isolates and Modeling isolation efficacy with large-scale dilution-to-extinction cultivation. *Appl Environ Microbiol* 2020; **86**:e00943-20. <https://doi.org/10.1128/AEM.00943-20>
19. Henson MW, Pitre DM, Weckhorst JL. et al. Artificial seawater media facilitate cultivating members of the microbial majority from the Gulf of Mexico. *mSphere* 2016; **1**:e00028-16.
20. Schäfer H, Servais P, Muyzer G. Successional changes in the genetic diversity of a marine bacterial assemblage during confinement. *Arch Microbiol* 2000; **173**:138–45. <https://doi.org/10.1007/s002039900121>
21. Edgar RC. MUSCLE: multiple sequence alignment with high accuracy and high throughput. *Nucleic Acids Res* 2004; **32**:1792–7. <https://doi.org/10.1093/nar/gkh340>
22. Capella-Gutiérrez S, Silla-Martínez JM, Gabaldón T. trimAl: a tool for automated alignment trimming in large-scale phylogenetic analyses. *Bioinformatics* 2009; **25**:1972–3. <https://doi.org/10.1093/bioinformatics/btp348>
23. Minh BQ, Schmidt HA, Chernomor O. et al. IQ-TREE 2: new models and efficient methods for phylogenetic inference in the genomic era. *Mol Biol Evol* 2020; **37**:1530–34.
24. Bolger AM, Lohse M, Usadel B. Trimmomatic: a flexible trimmer for Illumina sequence data. *Bioinformatics* 2014; **30**:2114–20. <https://doi.org/10.1093/bioinformatics/btu170>
25. Wick RR, Judd LM, Holt KE. Performance of neural network basecalling tools for Oxford Nanopore sequencing. *Genome Biol* 2019; **20**:129. <https://doi.org/10.1186/s13059-019-1727-y>
26. Kolmogorov M, Yuan J, Lin Y. et al. Assembly of long, error-prone reads using repeat graphs. *Nat Biotechnol* 2019; **37**:540–6. <https://doi.org/10.1038/s41587-019-0072-8>
27. Li H. Minimap and miniasm: fast mapping and de novo assembly for noisy long sequences. *Bioinformatics* 2016; **32**:2103–10. <https://doi.org/10.1093/bioinformatics/btw152>
28. Wick RR, Holt KE. Polypolish: short-read polishing of long-read bacterial genome assemblies. *PLoS Comput Biol* 2022; **18**:e1009802. <https://doi.org/10.1371/journal.pcbi.1009802>
29. Wick RR, Schultz MB, Zobel J. et al. Bandage: interactive visualization of de novo genome assemblies. *Bioinformatics* 2015; **31**:3350–2. <https://doi.org/10.1093/bioinformatics/btv383>
30. Mak SST, Gopalakrishnan S, Carøe C. et al. Comparative performance of the BGISEQ-500 vs Illumina HiSeq2500 sequencing platforms for palaeogenomic sequencing. *Gigascience* 2017; **6**:1–13. <https://doi.org/10.1093/gigascience/gix049>
31. Chen Y, Nie F, Xie S-Q. et al. Efficient assembly of nanopore reads via highly accurate and intact error correction. *Nat Commun* 2021; **12**:60. <https://doi.org/10.1038/s41467-020-20236-7>
32. Vaser R, Sović I, Nagarajan N. et al. Fast and accurate de novo genome assembly from long uncorrected reads. *Genome Res* 2017; **27**:737–46. <https://doi.org/10.1101/gr.214270.116>
33. Walker BJ, Abeel T, Shea T. et al. Pilon: an integrated tool for comprehensive microbial variant detection and genome

assembly improvement. *PLoS One* 2014;9:e112963. <https://doi.org/10.1371/journal.pone.0112963>

34. Sunagawa S, Acinas SG, Bork P. et al. Tara oceans: towards global ocean ecosystems biology. *Nat Rev Microbiol* 2020;18: 428–45. <https://doi.org/10.1038/s41579-020-0364-5>

35. Royo-Llonch M, Sánchez P, Ruiz-González C. et al. Compendium of 530 metagenome-assembled bacterial and archaeal genomes from the polar Arctic Ocean. *Nat Microbiol* 2021;6: 1561–74. <https://doi.org/10.1038/s41564-021-00979-9>

36. Larkin AA, Garcia CA, Garcia N. et al. High spatial resolution global ocean metagenomes from bio-GO-SHIP repeat hydrography transects. *Scientific Data* 2021;8:1–6. <https://doi.org/10.1038/s41597-021-00889-9>

37. Nishimura Y, Yoshizawa S. The OceanDNA MAG catalog contains over 50,000 prokaryotic genomes originated from various marine environments. *Scientific Data* 2022;9:305–11. <https://doi.org/10.1038/s41597-022-01392-5>

38. Silvano E, Yang M, Wolterink M. et al. Lipidomic analysis of roseobacters of the pelagic RCA cluster and their response to phosphorus limitation. *Front Microbiol* 2020;11:552135. <https://doi.org/10.3389/fmicb.2020.552135>

39. Chaumeil P-A, Mussig AJ, Hugenholtz P. et al. GTDB-Tk: a toolkit to classify genomes with the genome taxonomy database. *Bioinformatics* 2020;36:1925–27.

40. Olm MR, Brown CT, Brooks B. et al. dRep: a tool for fast and accurate genomic comparisons that enables improved genome recovery from metagenomes through de-replication. *ISME J* 2017;11:2864–8. <https://doi.org/10.1038/ismej.2017.126>

41. Parks DH, Imelfort M, Skennerton CT. et al. CheckM: assessing the quality of microbial genomes recovered from isolates, single cells, and metagenomes. *Genome Res* 2015;25:1043–55. <https://doi.org/10.1101/gr.186072.114>

42. Tria FDK, Landan G, Dagan T. Phylogenetic rooting using minimal ancestor deviation. *Nat Ecol Evol* 2017;1:193. <https://doi.org/10.1038/s41559-017-0193>

43. Jain C, Rodriguez-R LM, Phillippe AM. et al. High throughput ANI analysis of 90K prokaryotic genomes reveals clear species boundaries. *Nat Commun* 2018;9:5114. <https://doi.org/10.1038/s41467-018-07641-9>

44. Murat Eren A, Esen ÖC, Quince C. et al. Anvi'o: an advanced analysis and visualization platform for 'omics data. *PeerJ* 2015;3:e1319. <https://doi.org/10.7717/peerj.1319>

45. Kanehisa M, Sato Y, Morishima K. BlastKOALA and GhostKOALA: KEGG tools for functional characterization of genome and metagenome sequences. *J Mol Biol* 2016;428: 726–31. <https://doi.org/10.1016/j.jmb.2015.11.006>

46. Kanehisa M, Sato Y, Kawashima M. et al. KEGG as a reference resource for gene and protein annotation. *Nucleic Acids Res* 2016;44:D457–62. <https://doi.org/10.1093/nar/gkv1070>

47. Lanclos VC, Rasmussen AN, Kojima CY. et al. Ecophysiology and genomics of the brackish water adapted SAR11 subclade IIIa. *ISME J* 2023;17:620–9. <https://doi.org/10.1038/s41396-023-01376-2>

48. Graham ED, Heidelberg JF, Tully BJ. Potential for primary productivity in a globally-distributed bacterial phototroph. *ISME J* 2018;12:1861–6. <https://doi.org/10.1038/s41396-018-0091-3>

49. Emms DM, Kelly S. OrthoFinder: phylogenetic orthology inference for comparative genomics. *Genome Biol* 2019;20:238. <https://doi.org/10.1186/s13059-019-1832-y>

50. Kieft B, Li Z, Bryson S. et al. Microbial community structure-function relationships in Yaquina Bay estuary reveal spatially distinct carbon and nitrogen cycling capacities. *Front Microbiol* 2018;9:1282. <https://doi.org/10.3389/fmicb.2018.01282>

51. Damashek J, Edwardson CF, Tolar BB. et al. Coastal Ocean metagenomes and curated metagenome-assembled genomes from marsh landing, Sapelo Island (Georgia, USA). *Microbiol Resour Announc* 2019;8:e00934-19. <https://doi.org/10.1128/MRA.00934-19>

52. Sieradzki ET, Morando M, Fuhrman JA. Metagenomics and quantitative stable isotope probing offer insights into metabolism of polycyclic aromatic hydrocarbon degraders in chronically polluted seawater. *mSystems* 2021;6:e00245-21. <https://doi.org/10.1128/mSystems.00245-21>

53. Sieradzki ET, Fuhrman JA, Rivero-Calle S. et al. Proteorhodopsins dominate the expression of phototrophic mechanisms in seasonal and dynamic marine picoplankton communities. *PeerJ* 2018;6:e5798. <https://doi.org/10.7717/peerj.5798>

54. Alneberg J, Bennke C, Beier S. et al. Ecosystem-wide metagenomic binning enables prediction of ecological niches from genomes. *Commun Biol* 2020;3:119. <https://doi.org/10.1038/s42003-020-0856-x>

55. Alneberg J, Sundh J, Bennke C. et al. BARM and BalticMicrobeDB, a reference metagenome and interface to meta-omic data for the Baltic Sea. *Sci Data* 2018;5:180146. <https://doi.org/10.1038/sdata.2018.146>

56. Ahmed MA, Lim SJ, Campbell BJ. Metagenomes, Metatranscriptomes, and metagenome-assembled genomes from Chesapeake and Delaware Bay (USA) water samples. *Microbiol Resour Announc* 2021;10:e0026221. <https://doi.org/10.1128/MRA.00262-21>

57. Sakowski EG, Arora-Williams K, Tian F. et al. Interaction dynamics and virus-host range for estuarine actinophages captured by epicPCR. *Nat Microbiol* 2021;6:630–42. <https://doi.org/10.1038/s41564-021-00873-4>

58. Fortunato CS, Crump BC. Microbial gene abundance and expression patterns across a river to ocean salinity gradient. *PLoS One* 2015;10:e0140578. <https://doi.org/10.1371/journal.pone.0140578>

59. Di Cesare A, Dzhembekova N, Cabello-Yeves PJ. et al. Genomic comparison and spatial distribution of different *Synechococcus* phylotypes in the Black Sea. *Front Microbiol* 2020;11:1979. <https://doi.org/10.3389/fmicb.2020.01979>

60. Thrash JC, Seitz KW, Baker BJ. et al. Metabolic roles of uncultivated Bacterioplankton lineages in the northern Gulf of Mexico 'dead zone'. *MBio* 2017;8:e01017-7. <https://doi.org/10.1128/mBio.01017-17>

61. Xu B, Li F, Cai L. et al. A holistic genome dataset of bacteria, archaea and viruses of the Pearl River estuary. *Scientific Data* 2022;9:1–9. <https://doi.org/10.1038/s41597-022-01153-4>

62. Rasmussen AN, Francis CA. Genome-resolved metagenomic insights into massive seasonal ammonia-oxidizing archaea blooms in San Francisco Bay. *mSystems* 2022;7:e0127021. <https://doi.org/10.1128/msystems.01270-21>

63. Mende DR, Bryant JA, Aylward FO. et al. Environmental drivers of a microbial genomic transition zone in the ocean's interior. *Nat Microbiol* 2017;2:1367–73. <https://doi.org/10.1038/s41564-017-0008-3>

64. Kopf A, Bicak M, Kottmann R. et al. The ocean sampling day consortium. *Gigascience* 2015;4:27. <https://doi.org/10.1186/s13742-015-0066-5>

65. Tragin M, Vaulot D. Green microalgae in marine coastal waters: the ocean sampling day (OSD) dataset. *Sci Rep* 2018;8:14020. <https://doi.org/10.1038/s41598-018-32338-w>

66. Acinas SG, Sánchez P, Salazar G. et al. Deep ocean metagenomes provide insight into the metabolic architecture

of bathypelagic microbial communities. *Commun Biol* 2021;4:604. <https://doi.org/10.1038/s42003-021-02112-2>

67. Biller SJ, Berube PM, Dooley K. et al. Marine microbial metagenomes sampled across space and time. *Sci Data* 2018;5:180176. <https://doi.org/10.1038/sdata.2018.176>

68. Sunagawa S, Coelho LP, Chaffron S. et al. Ocean plankton. Structure and function of the global ocean microbiome. *Science* 2015;348:1261359. <https://doi.org/10.1126/science.1261359>

69. Kojima CY, Getz EW, Cameron TJ. RRAP: RPKM recruitment analysis pipeline. *Microbiology Resource Announcements* 2022;9:e00644-22.

70. Langmead B, Salzberg SL. Fast gapped-read alignment with bowtie 2. *Nat Methods* 2012;9:357-9. <https://doi.org/10.1038/nmeth.1923>

71. Danecek P, Bonfield JK, Liddle J. et al. Twelve years of SAM-tools and BCFtools. *Gigascience* 2021;10:giab008. <https://doi.org/10.1093/gigascience/giab008>

72. Aroney STN, Newell RJP, Nissen JN. et al. CoverM: read alignment statistics for metagenomics. *Bioinformatics* 2025;41:btaf147. <https://doi.org/10.1093/bioinformatics/btaf147>

73. Lewis E. The practical salinity scale 1978 and its antecedents. *IEEE J Ocean Eng* 1980;5:3-8. <https://doi.org/10.1109/JOE.1980.1145448>

74. Cho J-C, Giovannoni SJ. Cultivation and growth characteristics of a diverse group of oligotrophic marine Gammaproteobacteria. *Appl Environ Microbiol* 2004;70:432-40. <https://doi.org/10.1128/AEM.70.1.432-440.2004>

75. Cheng C, Thrash JC. Sparse-growth-curve: a computational pipeline for parsing cellular growth curves with low temporal resolution. *Microbiol Resour Announc* 2021;10:e00296-21.

76. Chen Y-B, Zehr JP, Mellon M. Growth and nitrogen fixation of the DIAZOTROPHIC filamentous NONHETEROCYSTOUS cyanobacterium TRICHODESMIUM SP.IMS 101 IN defined media: evidence for a circadian RHYTHM<sup>1</sup>. *J Phycol* 1996;32:916-23. <https://doi.org/10.1111/j.0022-3646.1996.00916.x>

77. Ritchie RJ. Measurement of chlorophylls a and b and bacteriochlorophyll a in organisms from hypereutrophic auxinic waters. *J Appl Phycol* 2018;30:3075-87. <https://doi.org/10.1007/s10811-018-1431-4>

78. Clifford EL, Varela MM, De Corte D. et al. Taurine is a major carbon and energy source for marine prokaryotes in the North Atlantic Ocean off the Iberian peninsula. *Microb Ecol* 2019;78:299-312. <https://doi.org/10.1007/s00248-019-01320-y>

79. Carini P, White AE, Campbell EO. et al. Methane production by phosphate-starved SAR11 chemoheterotrophic marine bacteria. *Nat Commun* 2014;5:4346. <https://doi.org/10.1038/ncomms5346>

80. Repeta DJ, Ferrón S, Sosa OA. et al. Marine methane paradox explained by bacterial degradation of dissolved organic matter. *Nat Geosci* 2016;9:884-7. <https://doi.org/10.1038/ngeo2837>

81. Malard LA, Guisan A. Into the microbial niche. *Trends Ecol Evol* 2023;38:936-45.

82. Colwell RK, Rangel TF. Hutchinson's duality: the once and future niche. *Proc Natl Acad Sci USA* 2009;106:19651-8. <https://doi.org/10.1073/pnas.0901650106>

83. Smith AN, Hennon GMM, Zinser ER. et al. Comparing Prochlorococcus temperature niches in the lab and across ocean basins. *Limnol Oceanogr* 2021;66:2632-47. <https://doi.org/10.1002/lno.11777>

84. Getz EW, Lanclos VC, Kojima CY. et al. The AEGEAN-169 clade of bacterioplankton is synonymous with SAR11 subclade V (HIMB59) and metabolically distinct. *mSystems* 2023;8:e0017923. <https://doi.org/10.1128/msystems.00179-23>

85. González JM, Kiene RP, Moran MA. Transformation of sulfur compounds by an abundant lineage of marine bacteria in the  $\alpha$ -subclass of the class Proteobacteria. *Appl Environ Microbiol* 1999;65:3810-9. <https://doi.org/10.1128/AEM.65.9.3810-3819.1999>

86. Feng X, Xing P. Genomics of Yoonia sp. isolates (family Roseobacteraceae) from lake zhangnai on the Tibetan plateau. *Microorganisms* 2023;11:2817. <https://doi.org/10.3390/microorganisms11112817>

87. Dong C, Idica EY, McWilliams JC. Circulation and multiple-scale variability in the Southern California bight. *Prog Oceanogr* 2009;82:168-90. <https://doi.org/10.1016/j.pocean.2009.07.005>

88. Hickey BM, Dobbins EL, Allen SE. Local and remote forcing of currents and temperature in the Central Southern California bight. *Journal of Geophysical Research: Oceans* 2003;108:3081. <https://doi.org/10.1029/2000JC000313>

89. National Centers for Environmental Information, National Oceanic and Atmospheric Administration. Coastal Water Temperature Guide. <https://www.ncei.noaa.gov/products/coastal-water-temperature-guide> (10 May 2024, date last accessed).

90. Kuo Y-C, Chan J-W, Wang Y-C. et al. Long-term observation on sea surface temperature variability in the Taiwan Strait during the northeast monsoon season. *Int J Remote Sens* 2018;39:4330-42. <https://doi.org/10.1080/01431161.2017.1387311>

91. Wang X, Xie M, Ho KEY. et al. A neutral process of genome reduction in marine bacterioplankton. *bioRxiv* 2024;2024.02.04.578831. <https://doi.org/10.1101/2024.02.04.578831>.

92. Liu Y, Brinkhoff T, Berger M. et al. Metagenome-assembled genomes reveal greatly expanded taxonomic and functional diversification of the abundant marine Roseobacter RCA cluster. *Microbiome* 2023;11:1-18. <https://doi.org/10.1186/s40168-023-01644-5>

93. Giebel H-A, Kalhoefer D, Gahl-Janssen R. et al. Planktomarina temperata gen. Nov., sp. nov., belonging to the globally distributed RCA cluster of the marine Roseobacter clade, isolated from the German Wadden Sea. *Int J Syst Evol Microbiol* 2013;63:4207-17. <https://doi.org/10.1099/ijst.0.053249-0>

94. Mayali X, Franks PJS, Azam F. Cultivation and ecosystem role of a marine Roseobacter clade-affiliated cluster bacterium. *Appl Environ Microbiol* 2008;74:2595-603. <https://doi.org/10.1128/AEM.02191-07>

95. Zhang Z, Chen F, Chu X. et al. Diverse, abundant, and novel viruses infecting the marine Roseobacter RCA lineage. *mSystems* 2019;4:e00494-19. <https://doi.org/10.1128/msystems.00494-19>

96. Durham BP, Grote J, Whittaker KA. et al. Draft genome sequence of marine alphaproteobacterial strain HIMB11, the first cultivated representative of a unique lineage within the Roseobacter clade possessing an unusually small genome. *Stand Genomic Sci* 2014;9:632-45. <https://doi.org/10.4056/sigs.4998989>

97. Giebel H-A, Wolterink M, Brinkhoff T. et al. Complementary energy acquisition via aerobic anoxygenic photosynthesis and carbon monoxide oxidation by Planktomarina temperata of the Roseobacter group. *FEMS Microbiol Ecol* 2019;95:fiz050. <https://doi.org/10.1093/femsec/fiz050>

98. Malfatti F, Samo TJ, Azam F. High-resolution imaging of pelagic bacteria by atomic force microscopy and implications for carbon cycling. *ISME J* 2010;4:427-39. <https://doi.org/10.1038/ismej.2009.116>

99. Henson MW, Lanclos VC, Faircloth BC. et al. Cultivation and genomics of the first freshwater SAR11 (LD12) isolate. *ISME J* 2018;12:1846-60. <https://doi.org/10.1038/s41396-018-0092-2>

100. Zhao X, Schwartz CL, Pierson J. et al. Three-dimensional structure of the Ultraoligotrophic marine bacterium 'Candidatus Pelagibacter ubique'. *Appl Environ Microbiol* 2017; **83**:e02807-16. <https://doi.org/10.1128/AEM.02807-16>

101. Kulichevskaya IS, Ivanova AA, Detkova EN. et al. Planctomicrobium piriforme gen. Nov., sp. nov., a stalked planctomycete from a littoral wetland of a boreal lake. *Int J Syst Evol Microbiol* 2015; **65**:1659-65. <https://doi.org/10.1099/ijsm.0.000154>